JOURNAL OF MATERIALS SCIENCE 20 (1985) 213–228

A microstructural study of local melting of grey cast iron by a static plasma arc

T. ISHIDA
Department of Metallurgical Chemistry, The Research Institute for Iron, Steel and Other Metals, Tohoku University, Sendai, Japan

The microstructural changes produced by plasma arc local-melting method in the fusion region or deposited metal, fusion boundary region and heat-affected zone (HAZ) of flake graphite cast iron were investigated. Cylindrical base metal specimens were locally melted at fixed time intervals under a stationary plasma torch using argon plasma gas and Ar + 10% H_2 shielding gas. The welds were produced autogenously and with filler metals. The cooling rate in the fusion region was recorded. Evaluation of the fusion boundary area included metallurgical analysis, microhardness and electron probe microanalysis. In the absence of filler metal, the structure of fusion region where completely melted was ledeburite. In the centre of the fusion region the structure appears to be that of hypoeutectic white cast iron, and in the fusion boundary of this region the structure appears to be fined ledeburite. In the fusion boundary region where supercooled phenomena can occur, fine martensite precipitates appear along the fusion line for small heat input and secondary graphite is seen for large heat input. The HAZ is composed of white martensitic, dark martensitic and martensitic–fine pearlitic layers for small heat input, and of finely laminated pearlitic and finely laminated pearlitic–ferritic layers for large heat input. Using filler metal, the structure of the deposited metal is found to be that of a nickel austenitic matrix precipitating tiny graphite nodules or slim graphite for nickel and Ni–Fe filler metals, but to be a pearlitic matrix for iron filler metal. In the fusion boundary region, nickel-martensite, eutectic or slim graphite and fine nickel-martensite are precipitated from the nickel system filler metal, and the columnar structure of ferrite and pearlite is obtained from iron filler metal. The HAZ is composed of thin ledeburitic, martensitic, martensitic–fine pearlitic and finely laminated pearlitic layers for the nickel filler metal, of ledeburitic and finely laminated pearlitic layers for the Ni–Fe filler metal, and of thick ledeburitic, eutectic graphite–crystallized and finely laminated pearlitic layers for iron filler metal. The hardness of the ledeburitic layer and the nickel–martensitic portion is very high where the liquid existed. The diffusion of nickel from the deposited metal into the HAZ can occur at least until the fused base metal of HAZ.

1. Introduction

It has recently been shown that the availability of high powered and continuous energy sources such as laser [1], electron beam [2, 3] and plasma arc [4] has led to the development of new materials processing techniques. One such process is a rapid melting and subsequent solidification of metallic substrates. In the present investigation a process of rapid surface melting and solidification due to a static heat flux of a high powered plasma arc was conducted for the application of grey cast iron to the weldment. It is anticipated that the utilization of plasma arc to weld or repair-weld large grey iron castings would be valid for the improvement of cast iron structures. The literature on grey iron welding is very scarce [5, 6] and little basic research on welding has been undertaken. In such a situation, recent studies by

0022–2461/85 $03.00 + .12

Devletian [7, 8], on the arc welding of grey cast iron using grey iron electrodes, have demonstrated that the weldability of grey iron is significantly affected by the cooling rate and carbon equivalent of the weld admixture, and that grey iron weld metal containing an optimum addition of aluminium exhibits a substantial graphitization and reduced hardness. In grey cast iron weldment the microstructure is characterized by the formation iron carbide and martensite in the heat-affected zone (HAZ). This iron carbide layer forms in the molten iron region of the fused and diluted base metal adjacent to the fusion region owing to the fast cooling rate. The formation of iron carbide may be avoided by adequate alteration of the chemical composition in the molten iron region. This variation is produced by the diffusion of deposit metal into the molten iron region in the HAZ. It is possible to make deposit metal diffuse until the molten iron region is reached, by the use of plasma arc [9]. The formation of martensite in the HAZ occurs in the portion immediately adjacent to this carbide region. Large amounts of carbon can be dissolved in austenite during the heating cycle by solution of carbon from flake graphite, and on rapid cooling, high carbon martensite will form. This martensite formation is partially eliminated by a high preheating to lessen the cooling rate. However, dispersion of the martensite may be achieved by the use of the plasma arc and the choice of suitable filler metal.

The purpose of this study is to elucidate the microstructural changes in flake graphite cast iron (FGI) for discrete regions produced by local melting under a static plasma arc, and thus to establish a sound mechanism for the origin of the fusion boundary deposited by nickel, Ni–Fe and iron filler metals in order to gain a better understanding of the basic plasma arc welding of grey cast iron. Specifically, this paper relates the interfacial microstructures of the fusion boundary and HAZ, with microhardness and diffusion on components across the fusion boundary.

2. Experimental method

The chemical composition of FGI used in these experiments is given in Table I. FGI was produced by reducing melting [10] steel scrap added to pig iron, in an electric furnace. The molten iron was cast into a sand mould 40 mm diameter. The predominant microstructure in these casting is a pearlitic matrix with flake graphite. Castings were cut into the specimen cylinders 35 mm diameter and 25 mm long. The filler metals used were provided from 10 mm diameter metal mould castings with deoxidized and degassed vacuum-melting of electrolytic nickel and iron. The filler metals were forged and rolled into wire rod of 4 mm diameter and 200 mm long. Commercial welding rods, CIA-1, 2 were also employed.

The heat source for the local arc-melting method was a transferred plasma arc welder (Hitachi, 300 A) with normal polarity. The base metal cylinder placing at the copper plate (15 mm x 100 mm x 100 mm) situated on the iron table was melted locally under the stationary plasma torch at fixed time intervals [9]. When filler metal was used, it was inserted into the plasma arc and deposited onto the base metal. Arc time measurement was done simultaneously with the transfer of the main arc. Plasma arc-time, i.e. the time over which the main arc occurred was from 10 to 40 sec, the welding current was 130 A, the plasma gas was argon with a flow rate of 2.8 $dm^3\ min^{-1}$ and the shielding gas was Ar + 10% H_2, with a flow rate of 13.0 $dm^3\ min^{-1}$. The electrode used was tungsten of 6.0 mm diameter and a nozzle diameter of 3.0 mm. The distance from the nozzle to the base metal was 8 to 10 mm. The shielding gas flowed out continuously a fixed time after the disappearance of the arc. Local-melting with or without filler metal was then carried out and the specimens were cooled to room temperature on the iron table, cross-sectioned, polished and then etched in 5% nital. Those with filler metal deposit were analysed across the deposited fusion boundary region using electron probe microanalysis (EPMA) and Vickers microhardness, H_v, test.

The temperature was measured to obtain the cooling curves of the melted region by plunging a 0.5 mm diameter Pt/Pt–13% Rh thermocouple directly into the molten pool immediately after

TABLE I Chemical composition of FGI (wt %)

	C	Si	Mn	P	S	C.E.*	Matrix
Base metal	3.49	2.24	0.59	0.016	0.015	4.2	pearlite

*Carbon equivalent = %C + 0.3(%Si + %P)

the arc had disappeared. The cooling curves were recorded on a continuous chart recorder and the average cooling rate for each specimen was determined over the temperature range 1000 to 900° C. The value of the cooling rate obtained was 23° C sec^{-1} for an arc time of 15 sec, 20° C sec^{-1} for an arc time of 20 sec, 13.5° C sec^{-1} for an arc time of 30 sec, and 12.5° C sec^{-1} for an arc time of 35 sec.

3. Results

3.1. Absence of filler metal

A significant difference builds up on the boundary area structure arising from the duration of the plasma arc, i.e. from the quantity of heat input from the plasma arc. This phenomenon is thought to be due to the influence of cooling rate. The microstructural changes in the fusion region, fusion boundary region and HAZ of FGI produced by the magnitude of heat input are described in the following sections.

3.1.1. Small heat input

Fig. 1 shows the microstructure of the fusion boundary area of FGI for an arc-time of 15 sec when subjected to plasma arc local melting. As shown in Fig. 1a, the fusion region becomes white iron and the HAZ becomes martensitic. As the arc-time is very short and the heat input small, the region of the fusion is shallow and narrow and the cooling rate is very high. The cooling rate in this fusion region is 23.0° C sec^{-1}. In this case a rapidly cooled structure appears in the fusion region and the HAZ. This fusion boundary area produced by plasma arc local melting can contain the following three regions of interest.

1. Fusion region. Cast iron directly beneath the plasma arc is completely melted, and immediately after the arc disappears, the liquid is rapidly frozen as white iron containing massive iron carbide and pearlite without effective nuclei for graphite. Therefore, the structure in this region is ledeburite in the absence of graphite.

2. Fusion line. The demarcation between ledeburite and the martensitic matrix is the fusion line. As shown in Fig. 1b, fine martensites appear along the fusion line and the matrix adjacent to the fusion line is a "white" martensite structure surrounded by very fine pearlite. As shown in Figs. 1c and d, fine martensites surrounding thin flake graphite are numerous, adjacent to the ledeburite. The specimens produced by local arc-melting are susceptible to a rapid heating from the fusion region and to a rapid cooling from the base metal in the vicinity of the fusion line.

3. HAZ. This region has chiefly a martensitic matrix with flake graphite. The martensite becomes refined and very fine pearlite begins to appear in great amounts with increasing distance from the fusion line. This HAZ is composed of four major regions between the fusion line and the base metal.

(a) White martensite layer. Martensite adjacent to the fusion line is little etched, as shown in Fig. 1e, and this is termed white martensite which is considered to be a tetragonal martensite. Martensites immediately adjacent to flake graphite are etched and appear black and have a needle-like shape (Fig. 1f). As indicated in Fig. 1c, flake graphite in the vicinity of the fusion line becomes much thinner owing to dissolution and diffusion of carbon into the austenitic matrix during the heat cycle. In this region there is a large migration of carbon from flake graphite into austenite, and on rapid cooling high carbon austenite transforms into coarse martensite and the matrix immediately adjacent to flake graphite may be in the carbon-supersaturated state.

(b) Dark martensite layer. A short distance away from the fusion line, dark-etched and fine martensite is seen as shown in Fig. 1g. This martensite is similar to that characteristic of a short-time tempering, which is thought to be of a cubic martensite. Tetragonal martensite transforms to cubic martensite precipitating ϵ-carbide, therefore, the martensite is visible generally as black areas.

(c) Martensite–fine pearlite layer. Further away from the fusion line a large amount of fine pearlite appears in the neighbourhood of flake graphite. As shown in Fig. 1h, a structure formed by the mixing of fine martensite and fine pearlite is observed. Also in this region migration of carbon into the matrix can occur.

(d) Finely laminated pearlite structure. Pearlite in the matrix near the base metal becomes finely laminated. In this region carbon migration into the matrix has hardly occurred.

The average layer thickness and hardness of each region of the HAZ are given in Table II. The layer thickness is larger at the circumference of the bead than in the centre.

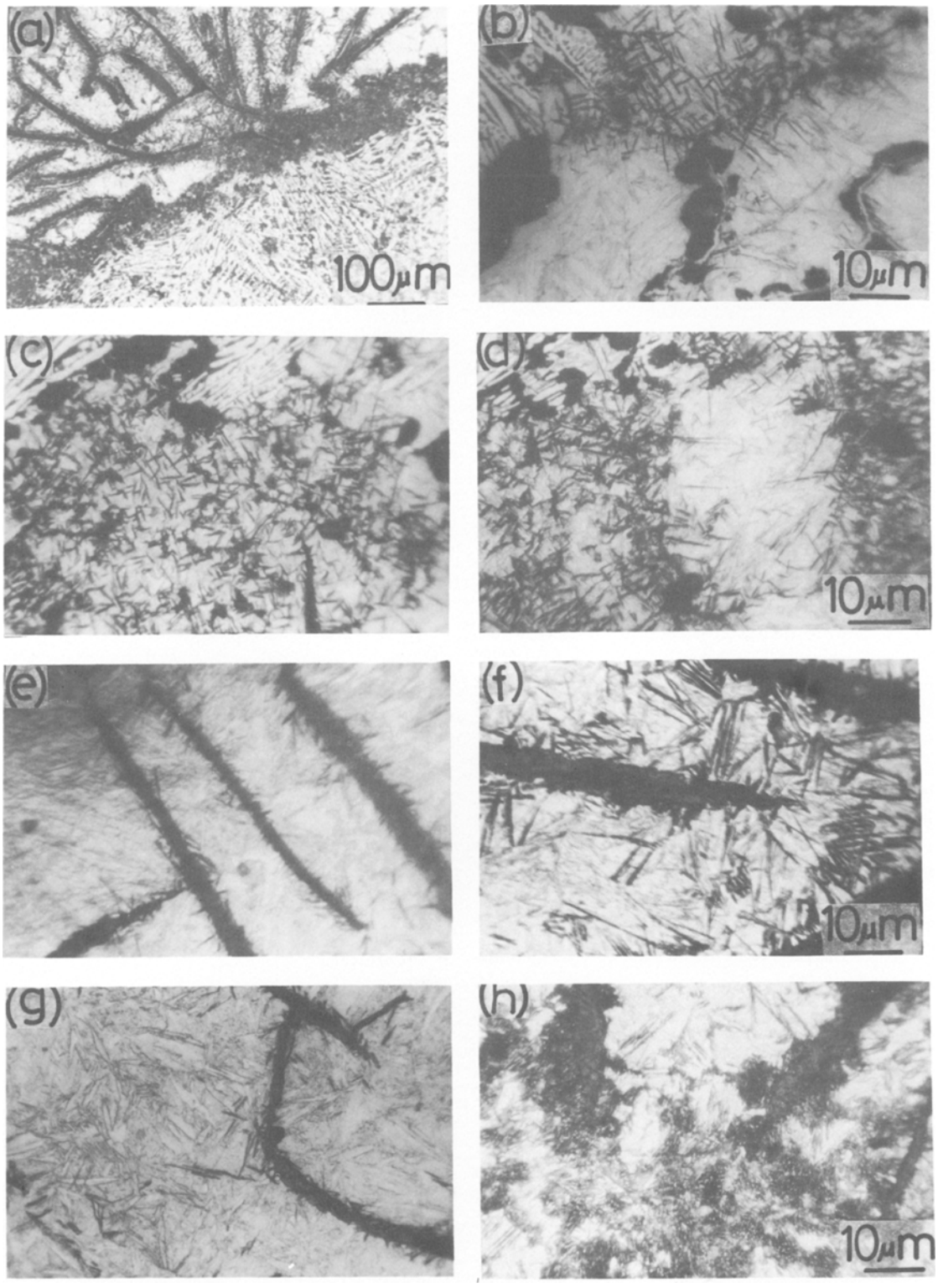

Figure 1 Microstructure of the fusion boundary and the HAZ of FGI after an arc-time of 15 sec produced by plasma arc local-melting using argon plasma gas and Ar + 10% H_2 shielding gas at an arc current of 130 A. Nital etch. (a) Fusion boundary area. (b) Fine martensites along the fusion line. (c), (d) Fine martensites surrounding slender flake graphite neighbouring ledeburite. (e) White martensite in the neighbourhood of the fusion line. (f) Black etched martensites bordering flake graphite. (g) Dark and fine martensites far from the fusion line. (h) Martensitic–fine pearlitic structure.

TABLE II Average thickness and hardness of each of the three layers in the HAZ after a plasmon arc-time of 15 sec

HAZ	Thickness of section of bead (mm)		Vickers microhardness, H_v
	Centre	Near to edge	
White martensite layer	0.186	0.295	677
Dark martensite layer	0.310	1.183	674
Martensite–fine pearlite layer	0.319	0.699	352

3.1.2. Large heat input

Fig. 2 shows the microstructure of the fusion boundary area of FGI for arc-time of 25 sec after plasma arc local melting. The cooling rate in this fusion region is 17.0° C sec^{-1}. As the heat input from the plasma arc becomes large for longer arc-times, the melted zone is enlarged and the temperature of the molten metal is increased. Therefore, the cooling rate in the fusion boundary and the HAZ is low, and a slowly cooled structure appears in each region. As shown in Fig. 2a, the fusion region becomes white iron, and the HAZ has a finely laminated pearlite structure. The microstructural changes of each region are described below.

1. Fusion region. As shown in Fig. 2b this region is white iron with massive iron carbide and eutectic. For a longer arc-time of 25 sec, a variation in the constituents of this region may occur. In the centre of the fusion region, the structure is thought to be that of hypoeutectic white cast iron, but in the fusion boundary of this region, fine ledeburite is obtained.

2. Fusion line. Demarcation between the fine ledeburite structure and the pearlitic one is the fusion line (Fig. 2c). As shown in Fig. 2d, flake graphite existing in the ledeburitic structure remains slender as undissolved graphite. Surrounding the slenderized graphite is a large amount of small graphite appearing in the pearlitic matrix outwards towards the ledeburite (Fig. 2e). Figs. 2f and g show graphite which was completely melted and small graphites which crystallized during solidification. The pearlite matrix containing these graphites is seen to adjoin the ledeburitic structure in Fig. 2h. These graphites are less numerous at the centre of the bead and become more numerous going out from the centre to both edges. The form of graphite flakes observed in the fusion line is similar to the interdendritic ASTM types D and E [11], however, the shape size is very small in comparison with that of D and E types.

3. HAZ. Greater heat from the melted zone obviates martensite formation in the HAZ. As described below, a finely laminated pearlitic structure is obtained in such a high preheat as to proceed.

(a) Finely laminated pearlite layer. The matrix is finely laminated with pearlite as shown in Fig. 2i and this layer becomes relatively thick.

(b) Laminated pearlite–ferrite mixed layer. A short distance away from the fusion line, ferrite appears in a position far away from the graphite flake. This ferrite exists only at a position where the diffusion of carbon has hardly occurred.

(c) Finely laminated pearlite layer. Pearlite becomes finely laminated and ferrite also exists.

The average thickness and microhardness of each layer in the HAZ obtained for a large heat input are given in Table III. Each layer is thicker at the circumference than in the centre, especially the finely laminated pearlite layer which becomes relatively thick at the circumference.

3.2. Use of filler metal

3.2.1. Nickel filler metal

Fig. 3 shows the microstructure of the deposited fusion boundary area of FGI formed by the plasma arc using nickel filler metal. The microstructural changes of each region are described below.

1. Deposited metal, DM. In this region Ni–Fe–C alloy is produced constituently, by the dilution of the base metal [12]. Tiny spheroidal

TABLE III Average thickness and hardness of each of the two layers in the HAZ after a plasma arc-time of 25 sec

HAZ	Thickness of section of bead (mm)		Vickers microhardness, H_v
	Centre	Near to edge	
Pearlite layer	1.6	1.8 ~ 3.55	431
Pearlite–ferrite layer	1.4	1.9	369

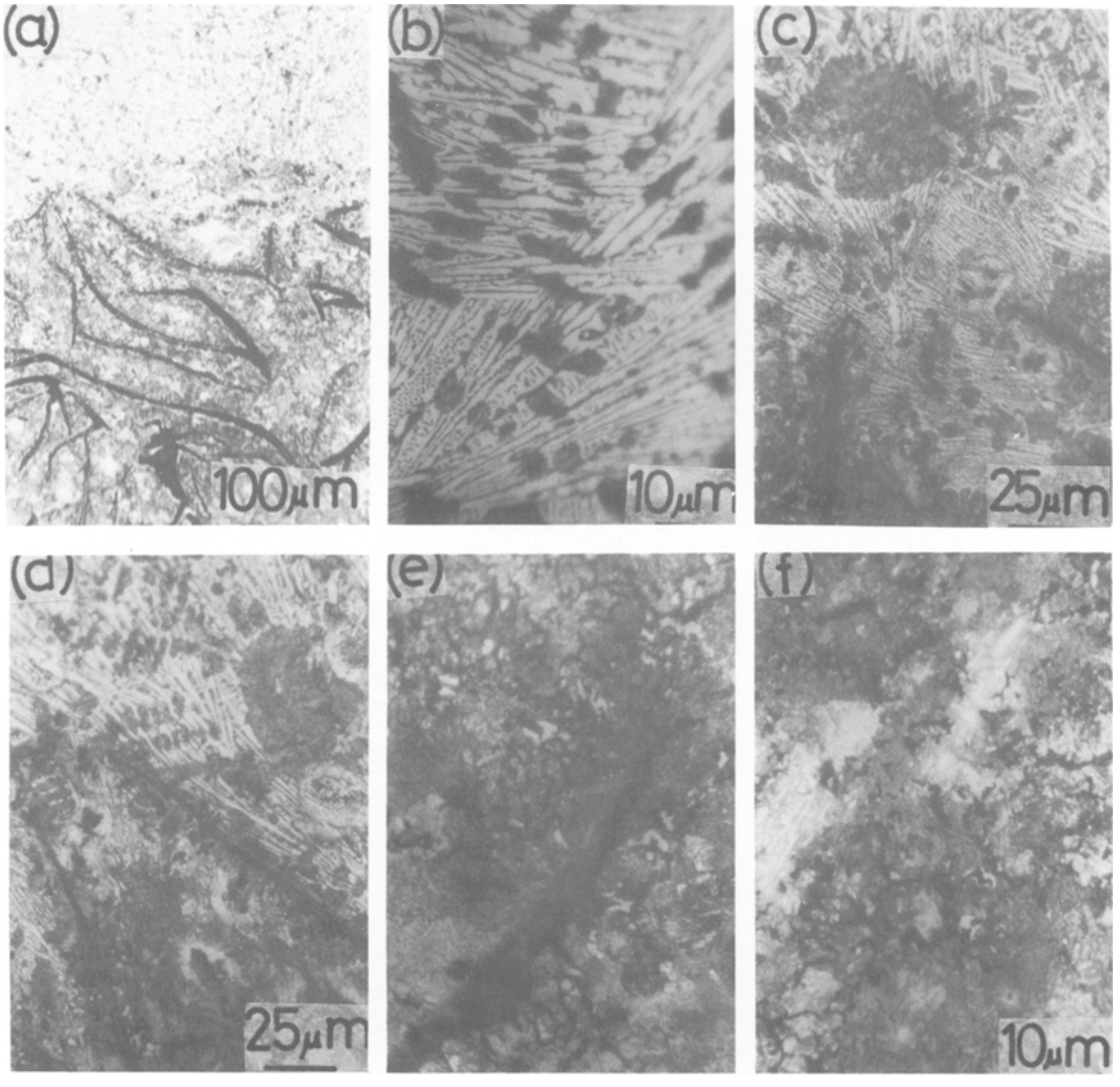

Figure 2 Microstructure of the fusion boundary and the HAZ of FGI after an arc-time of 25 sec produced by plasma arc local-melting using argon plasma gas and Ar + 10% H_2 shielding gas at an arc current of 130 A. Nital etch. (a) Fusion boundary area. (b) Ledeburite in fusion region. (c) Fusion line region between ledeburite and pearlite. (d) Slender graphites retained as non-fusion graphite in the ledeburitic region. (e) Tiny graphites precipitated during solidification from the liquid phase. (g) Tiny graphites precipitated in the neighbourhood of flake graphite. (h) Tiny graphites and pearlitic matrix in contact with ledeburite. (i) Flake graphite with finely laminated pearlite matrix at the HAZ.

graphite is crystallized within this region as indicated in Fig. 3a, and is particularly numerous in the vicinity of the fusion boundary. At locations in close proximity to the fusion boundary, graphite flakes are observed, as shown in Fig. 3b.

2. Fusion boundary region. In the centre and at both edges of the bead, nickel-martensite [13, 14] adjoins the ledeburitic structure as shown in Fig. 3c. At the circumference of the central region, as shown in Fig. 3d, small and tiny flake graphite–crystallized nickel alloy adjoins the eutectic graphite and fine nickel–martensite with the circumference of flake graphite remaining slender as undissolved graphite, which adjoins the base metal. Thus, in this fusion boundary region nickel–martensite [15], undercooled graphite, fine nickel–martensite and ledeburite are formed during rapid solidification.

3. HAZ. (a) Ledeburitic layer. A relatively thin layer of ledeburitic structure appears in the centre and at both edges of the bead, as shown in Fig. 3e. Moving from the centre towards the

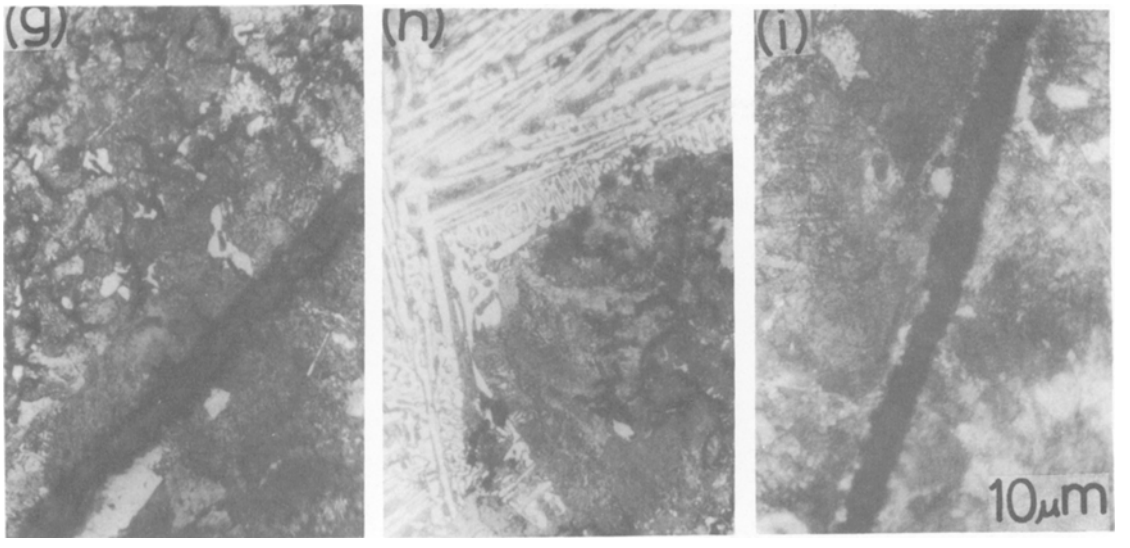

Figure 2 Continued

circumference the ledeburitic structure disappears. The portion where ledeburite appears is a partially melted region of the base metal caused by the heat from the deposit-metal side.

(b) Martensite layer. Martensite near the fusion line side is large needle-shaped. With increasing distance from the fusion line, the martensite becomes refined and a fine pearlite also exists. Martensite adjoining the ledeburite precipitates with fine pearlite around the boundary, as shown in Fig. 3f.

(c) Martensite–fine pearlite layer. Further away from the fusion line, martensite in addition to fine pearlite exists in great quantities, that is, mixing of martensite and fine pearlite is observed.

(d) Finely laminated pearlite layer. On approaching the base metal, the matrix becomes laminated with fine pearlite.

(e) Sorbitic pearlite layer. The pearlite in the base metal becomes very finely laminated.

3.2.2. Ni–Fe filler metal

3.2.2.1. 50 wt % Ni–50 wt % Fe filler metal. Fig. 4 shows the microstructure of the deposited fusion boundary area with 50 wt % Ni–50 wt % Fe filler metal.

1. DM. In this region Ni–Fe–C alloy is produced and tiny spheroidal graphite is crystallized within this region as shown in Fig. 4a, in particularly great amounts in the vicinity of the fusion boundary.

2. Fusion boundary region. In the centre of the bead, Ni–Fe martensite adjoins ledeburite as shown in Fig. 4b. In the range from the circumference to both edges of the bead, Ni–Fe martensite and the other link with a finely laminated pearlite matrix as shown in Fig. 4c. In the former, at the centre Ni–Fe alloy adjoins ledeburite and at the circumference Ni–Fe martensite adjoins ledeburite. The ledeburite grows on the Ni–Fe side and connects with Ni–Fe martensite. This martensite is a large bamboo leaf-like one. In the latter, Ni–Fe martensite is present as a mixture of the large bamboo leaf-like martensite and fine martensite, and eutectic graphite also precipitates, as shown in Fig. 4d. A great amount of eutectic graphite and fine martensite precipitates in a jumble, (Fig. 4e) and these adjoin the laminated pearlite matrix.

3. HAZ. (a) Ledeburitic layer. In the centre and at the edges of the bead, a ledeburitic layer appears as shown in Fig. 4f. At the circumference the layer is not recognizable.

(b) Finely laminated pearlite layer. The layer adjacent to the ledeburitic layer and the portion where ledeburite disappears have a finely laminated pearlite structure.

(c) Sorbitic pearlite layer. Pearlite in this layer becomes very finely laminated.

3.2.2.2. Commercial CIA-2 welding rod. Fig. 5 shows the microstructure of the deposited fusion boundary area of a CIA-2 (carbon-coated 55 wt % Ni–45 wt % Fe filler metal) welding rod. The structure of the fusion boundary is shown in Fig. 5a.

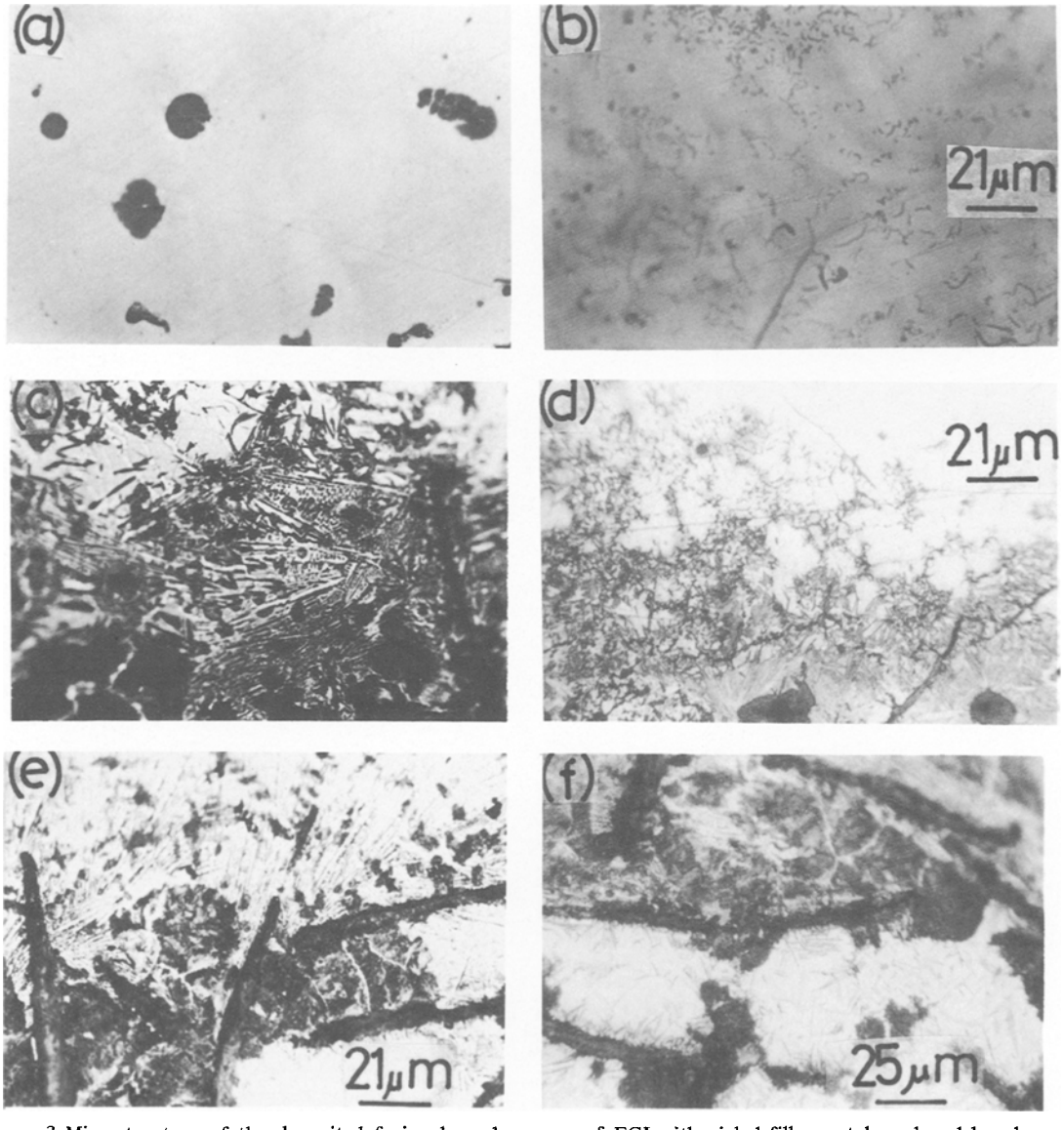

Figure 3 Microstructure of the deposited fusion boundary area of FGI with nickel filler metal produced by plasma arc using argon plasma gas and Ar + 10% H_2 shielding gas at an arc current of 130 A. Nital etch. (a) Tiny graphite nodules in a nickel austenitic matrix of deposit metal. (b) Tiny graphite flakes adjacent to the fusion boundary in the deposit metal. (c) Ledeburite adjoining the nickel–martensite in the fusion boundary region. (d) Eutectic graphite, fine nickel–martensite in the fusion boundary region. (e) Ledeburitic layer in the HAZ. (f) Martensitic layer in the HAZ.

1. DM. As can be seen in Fig. 5b, a eutectic–graphite network is precipitated in the Ni–Fe depositing region which contains a small amount of graphite nodules. This graphite network is thought to be net-shaped graphite formed by breakdown of Ni_3C.

2. Fusion boundary region. In the centre of the bead, Ni–Fe alloy adjoins the ledeburitic layer and approaching both edges, as shown in Fig. 5c, the nickel–martensite precipitates with eutectic graphite, and adjoins the finely laminated pearlite matrix of the cast iron base metal.

3. HAZ. The region partially melted by the heat from the deposit metal appears as ledeburitic structure during solidification and the non-fused portion becomes finely laminated pearlite.

(a) Ledeburitic layer. At the centre and at both edges of the bead, ledeburite appears.

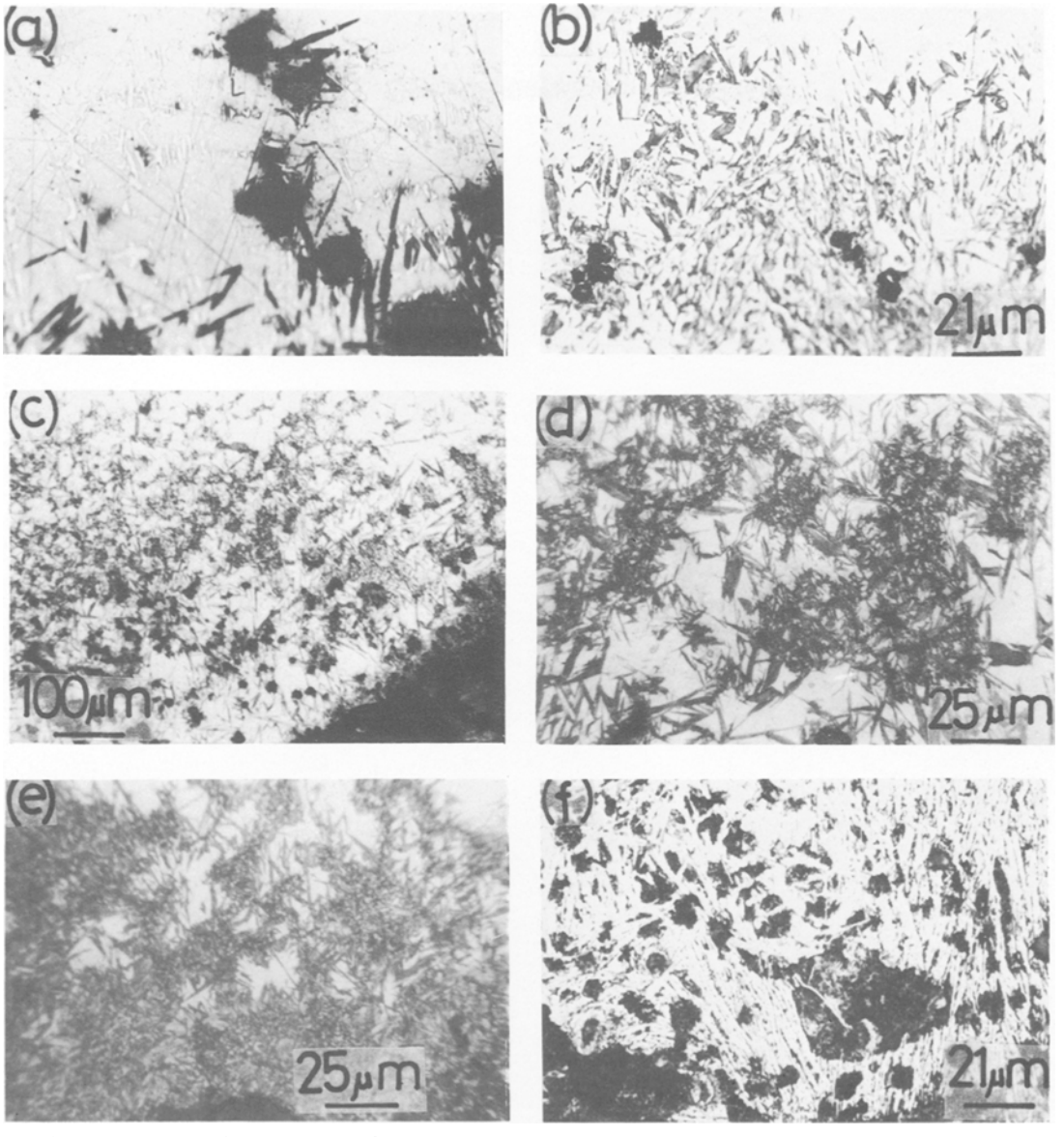

Figure 4 Microstructure of the deposited fusion boundary area of FGI with 50 wt% Ni–50 wt% Fe filler metal produced by plasma arc using argon plasma gas and Ar + 10% H_2 shielding gas at an arc current of 130 A. Nital etch. (a) Tiny spheroidal graphite in Ni–Fe alloy of the deposit metal. (b) Ni–Fe martensite adjoining ledeburite in the fusion boundary region. (c) Ni–Fe martensite, eutectic graphite in the fusion boundary region. (d) Large bamboo leaf-like Ni–Fe martensite and eutectic graphite in the fusion boundary region. (e) Fine Ni–Fe martensite and eutectic graphite adjoining finely laminated pearlite matrix in the fusion boundary region. (f) Ledeburitic layer in the HAZ.

(b) Laminated pearlite layer. The finely laminated pearlite layer exists thickly, having been measured to be about 1.4 mm at the centre and about 3.2 mm at both edges.

3.2.3. Iron filler metal

Fig. 6 shows the microstructure of the deposited fusion boundary area with iron filler metal. The structure of the deposit metal is pearlite and that of the fusion boundary is white iron, as shown in Fig. 6a.

1. DM. Fe–C–Si alloy is constituently formed in this region, and has a pearlite matrix.

2. Fusion boundary region. The boundary between pearlite in the iron side and ledeburite eutectic is the fusion line, as can be seen in Fig. 6b.

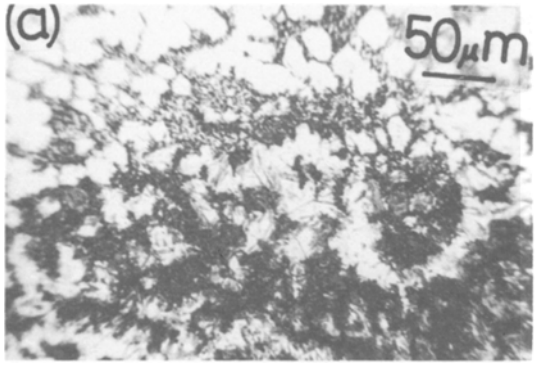

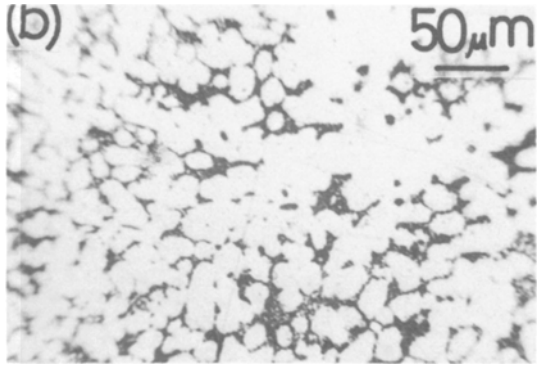

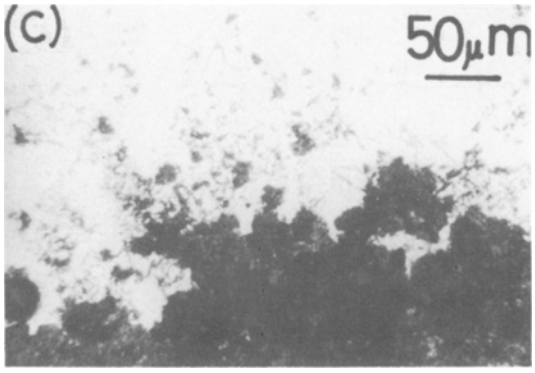

Figure 5 Microstructure of the fusion boundary of FGI deposited with CIA-2 (carbon-coated 55% Ni–45% Fe filler metal) welding rod produced by plasma arc using argon plasma gas and Ar + 10% H_2 shielding gas at an arc current of 130 A. Nital etch. (a) Deposit fusion boundary. (b) Eutectic graphite precipitated within the deposit metal. (c) Nickel–martensite in contact with the fine pearlite matrix.

As shown in Fig. 6c, the deposit metal in the vicinity of the fusion line is of a columnar crystal structure of ferrite and pearlite.

3. HAZ. (a) Ledeburite layer. A relatively thick ledeburitic layer usually appears along the fusion line, as shown in Fig. 6d.

(b) Eutectic graphite-crystallized layer. At the circumference and at both edges of the bead after a relatively slow cooling rate, eutectic graphite is crystallized and the layer may be clearly seen; however, at the centre of the bead it is not recognizable, as can be seen in Fig. 6e. The thickness of this layer which has a pearlitic matrix, is about 0.21 mm.

(c) Finely laminated layer. The base metal adjoining the ledeburitic layer or eutectic graphite–crystallized layer is very finely laminated pearlite.

(d) Laminated pearlite layer. Pearlite of the base metal becomes finely laminated.

3.2.4. Thickness of the ledeburitic layer

Average values of thickness of the ledeburitic layer in the HAZ for various filler metals are given in Table IV. The thickness of the ledeburitic layer varies with position and completely disappears in places. For the nickel system filler metal, the ledeburitic layer is thicker at the centre of the bead where the plasma flow is intense and is thin at both edges. However, using iron filler metal, the layer is thicker between the circumference and both edges than in the centre. Generally, the ledeburitic layer is thicker for iron filler metal than for the nickel system filler metal. This is thought to be due to the differences in melting point of the filler metal. Nickel and iron have higher freezing points than cast iron. In such a case, the melting of the base metal adjacent to the deposit metal proceeds during the course of freezing of the deposit metal, causing fusion forming ledeburitic eutectic layer. Accordingly, since the melting point of iron is higher than that of nickel and Ni–Fe, a large fusion of base metal cast iron occurs for iron filler metal and the ledeburitic layer subsequently appears thicker in the fused region.

3.2.5. Hardness across the deposit fusion boundary

Fig. 7 shows the results of the microhardness tests across deposit fusion boundary using nickel,

TABLE IV Average thickness of the ledeburitic layer in the HAZ using filler metals

Filler metal	Position in the section of bead (mm)	
	Centre	Edge
Ni	0.169	0.05
Ni–Fe	0.124	0.04
Fe	0.254	0.415

Ni–Fe and iron filler metals. The Vickers microhardness was measured with a load of 500 g, avoiding a fall into the graphite cavities. The hardness of nickel–martensite and Ni–Fe martensite was high, about VHN 675 and VHN 725, respectively, that of the ledeburitic layer was very high, about VHN 610 to 860 for nickel and Ni–Fe filler metals, but slightly lower (about VHN 490 and 530) for iron filler metal. In addition, the hardness was about VHN 550 in the martensitic area of the HAZ, VHN 450 in the martensitic–fine particles area and about VHN 400 to 450 in the finely laminated pearlite layer.

3.2.6. EPMA in the fusion boundary

Figs. 8 and 9 show the results of EPMA traces across the deposit fusion boundary using nickel and Ni–Fe filler metals. The diffusion layer about 0.2 mm thick can be recognized across the fusion line. The nickel content changes in the ledeburitic layer producing a concentration gradient. This indicates that nickel diffuses from the deposit metal into the HAZ.

4. Discussion

4.1. Absence of filler metal

Cast iron, where the plasma arc directly strikes, is completely melted and the liquid solidifies as

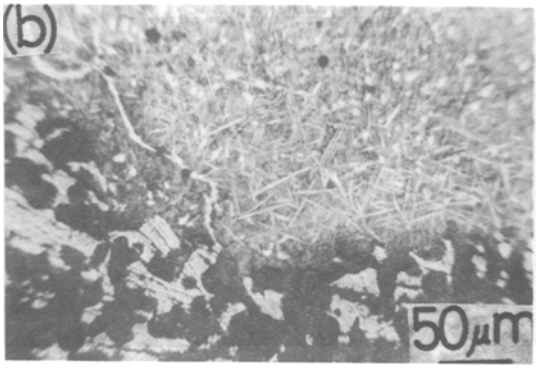

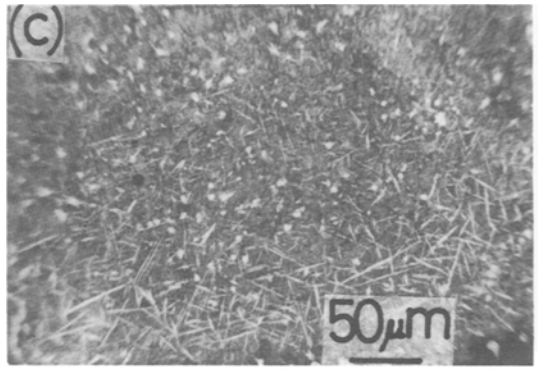

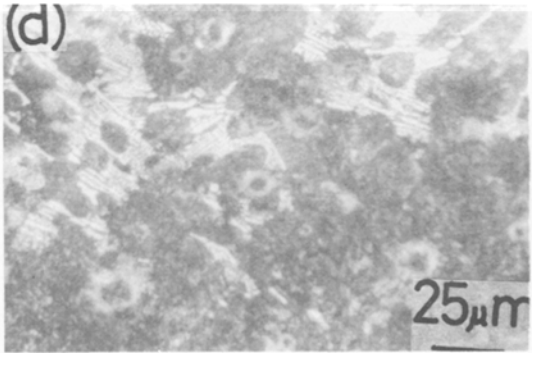

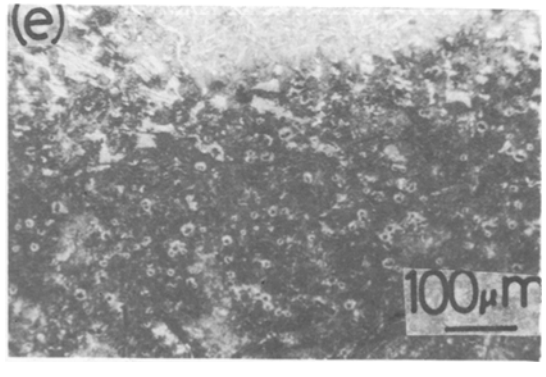

Figure 6 Microstructure of the fusion boundary and the HAZ of FGI deposited with iron filler metal by a plasma arc using argon plasma gas and Ar + 10% H_2 shielding gas at an arc current of 130 A. Nital etch. (a) Deposit fusion boundary region. (b) Fusion boundary region having ledeburite adjacent to pearlite on the iron deposit metal side. (c) Columnar structure consisting of ferrite and pearlite on the deposit metal side of the fusion boundary. (d) Ledeburitic layer in the HAZ. (e) Eutectic graphite layer appearing in the HAZ.

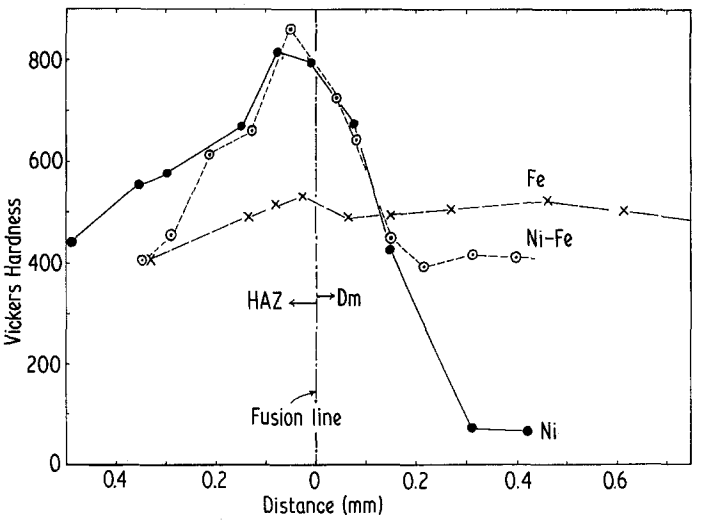

Figure 7 Hardness of FGI across the fusion boundary deposited with nickel, Ni–Fe and iron filler metals.

the ledeburite eutectic. In the centre of the fusion region the structure appears to be that of hypoeutectic white cast iron [16], but fined ledeburite in the vicinity of the fusion boundary is indistinguishable hypoeutectic from hypereutectic white cast iron. The formation of this ledeburite seems to be due to a rapid cooling effect, as no variation in the composition of the fusion region or a reaction with the plasma gas may occur in such a short arc-time. Furthermore, a larger heat input over long arc-times lowers the cooling rate, but as the rate is still very high in comparison with during casting, the major cause of the formation may be a relatively high cooling rate. In particular, the molten iron in the vicinity of the fusion boundary freezes as white iron, owing to an undercooling phenomenon. The increase in the temperature of the molten iron with increase in arc-time in this completely melted region allows a reaction with plasma shielding gas and a loss of carbon and silicon to occur [17]. In such a case, the cast iron in the fusion region becomes constituently hypoeutectic. In the fusion boundary region, the amount of crystallized graphite is, is smaller in the centre of the bead than at the circumference. This fact is related to the cooling rate during solidification, but the formation of graphite nuclei is thought to be avoided by agitation at the centre of the bead which is subjected to an intense plasma gas flow.

Fig. 10 shows a schematic illustration of the structure in the fusion boundary area of FGI produced by the plasma arc local-melting method without a filler metal. With a small heat input

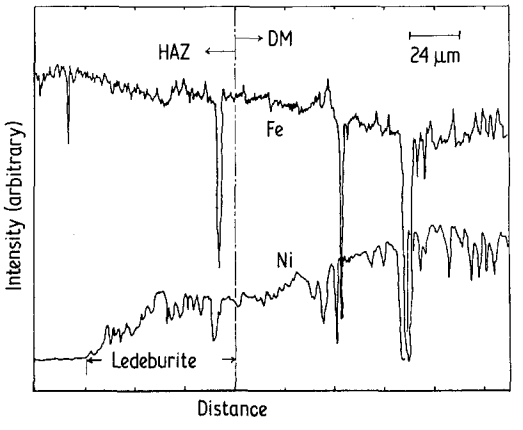

Figure 8 EPMA traces of Ni$K\alpha$ and Fe$K\alpha$ rays across the fusion boundary of FGI deposited with nickel filler metal by plasma arc using argon plasma gas and Ar + 10% H_2 shielding gas at an arc current of 130 A.

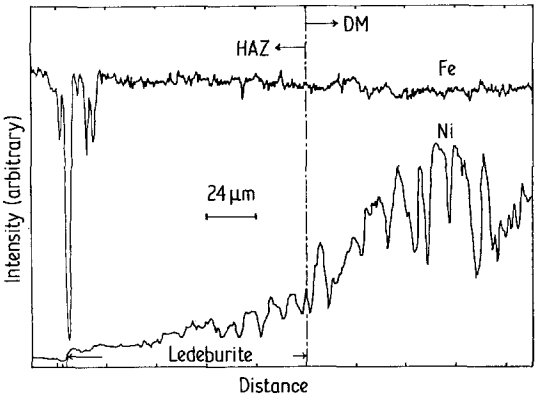

Figure 9 EPMA traces of Ni$K\alpha$ and Fe$K\alpha$ rays across the fusion boundary of FGI deposited with Ni–Fe filler metal by the plasma arc using argon plasma gas and Ar + 10% H_2 shielding gas at an arc current of 130 A.

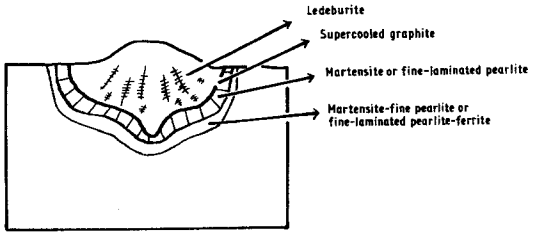

Figure 10 Schematic illustration of the structures of each region of FGI produced by plasma arc local-melting without a filler metal.

the structure in the HAZ is martensite, due to a high cooling rate. An especially fine martensite appears on the fusion line, which is considered to be a result of supercooling. Martensite in the HAZ consists of coarse α-martensite adjacent to the fusion line and fined β-martensite precipitating ϵ-carbide on the base metal side. Martensite is known to be easily decomposed under the M_s point [18]. This β-martensite is thought to be formed by the decomposition of α-martensite, thus the martensite in the base metal side is thought to be subjected to a short-time tempering. For a large heat input the fusion region becomes white cast iron; however, very small flake graphite appears in a portion of the molten iron in the vicinity of the fusion line, which seems to be precipitated as a secondary graphite during solidification. This secondary graphite is crystallized from the liquid phase, namely it is a supercooled graphite. Acquisition of a relatively low cooling rate on larger heat input preceeds graphitization in the vicinity of the fusion line and decreases the partial supersaturation of carbon into the austenitic matrix in the HAZ, causing the HAZ structure to become finely laminated pearlite.

A solid solution phenomenon with dissolution and diffusion of carbon from flake graphite into the austenitic matrix in the HAZ occurs greatly on approaching the fusion line. The range over which carbon solid solution occurs occupies the major part of the HAZ. The amount of solid solution is dependent upon heating temperature and holding time, and specific structures such as martensite, fine pearlite, finely laminated pearlite produced from the dependence on degree of solid solution of carbon and the magnitude of the cooling rate. The migration of carbon hardly occurs in these locations until a very finely laminated pearlite structure bordering the unaffected base metal appears. The carbon solid solution

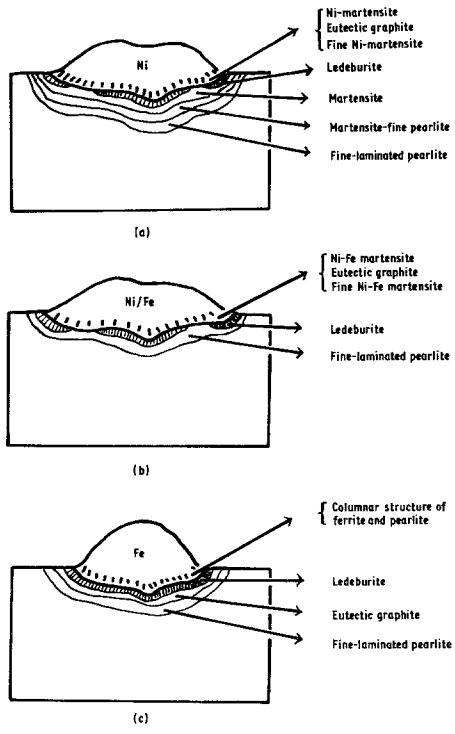

Figure 11 Schematic illustrations showing the structure of the fusion boundary area of FGI deposited with filler metals by a plasma arc. (a) Deposition with a nickel filler metal. (b) Deposition with Ni–Fe filler metal. (c) Deposition with iron filler metal.

process involves a dissolution reaction at the interface between graphite and the matrix, and a diffusion process of the carbon atom diffusing into the matrix. The rate of carbon solid solution has been reported to be controlled by the dissolution reaction [19]. It is pointed out from these results that the interfacial concentration between the flake graphite and the matrix cannot reach saturation. This indicates that the melting point of the matrix around the flake graphite is not unduly lowered. This is also understood from the fact that the matrix immediately adjacent to flake graphite shows no evidence of having fused and solidified as ledeburite eutectic.

4.2. Use of filler metal

Fig. 11 illustrates schematically the structures of the fusion boundary area of FGI deposited with a filler metal by a plasma arc. On the deposit metal side of the fusion boundary region, nickel–martensite (Figs. 3c, 4d), eutectic graphite (this is thought to be graphite which is partially decomposed by Ni_3C [20, 21]), fine nickel–martensite

(Fig. 3d), and small flake graphite (Figs. 3d, 4d) are precipitated with nickel and Ni–Fe filler metal, and needle-like ferrite (Figs. 6b, c) is precipitated with iron filler metal, which is recognized as a super-cooling effect in this region. The structure of the HAZ varies with the difference in melting point of the filler metal. Using nickel filler metal which has a melting point near to that of cast iron, as shown in Fig. 11a, the HAZ is composed of a relatively thin ledeburitic layer, martensitic layer, martensitic–fine pearlitic mixed layer and laminated pearlite layer. Using Ni–Fe filler metal, as shown in Fig. 11b, the HAZ consists of a ledeburitic layer and a laminated pearlite layer. Furthermore, using iron filler metal which has a relatively high melting point, a relatively large fused region of base metal is produced and the HAZ is composed of three layers, e.g. relatively thick ledeburitic, eutectic graphite–crystallized and laminated pearlitic, as indicated in Fig. 11c.

The hardness in the fusion boundary, namely at the nickel–martensite and ledeburitic layer, was very high where the liquid existed; however, with iron filler metal it was slightly lower in the ledeburitic area where diffusion of iron from the deposit metal occurred. Using iron filler metal, the hardness hardly changes in the fusion boundary.

With the use of a filler metal having a low melting point, the quantities of heat transfer from the deposit metal into the base metal and of the fused region of base metal, are relatively small. Consequently, the ledeburitic layer becomes thin and the martensitic layer in the HAZ is produced due to a rapid cooling. Using filler metal which has a high melting point, the amount of heat transfer from the deposit metal side becomes large and the ledeburitic layer in the HAZ becomes thick. In this case, martensite is not observed, but the layer crystallizes and eutectic graphite is formed. Generally, using filler metal, white iron layer with massive carbide is formed on the base metal side in the fusion boundary region. This carbide layer is thought to appear as a result of the fusion of base metal occurring during solidification of the deposit metal or subsequently. Thus the formation of white iron is an unsuitable feature for good welding. The structure of the HAZ can be controlled by the magnitude of the heat input from the arc and by the type of filler metal used. The use of filler metal having a melting point near to that of the base metal and a large heat input causes the white iron layer to thin or disappear, and to avert rapidly cooled martensite formation and partial supersaturation of carbon in the HAZ, i.e. using carbon-coated nickel filler metal CIA-1, and with a large heat input, the cooling rate in the fusion boundary area should be so slow as to render impossible the foundation of a white iron structure, but to produce a graphitized structure as described below.

The deposit metal has a nickel austenitic matrix containing many slim graphites as shown in Fig. 12a. In the fusion boundary region, at the centre of the bead, nickel–martensite (Fig. 12b) precipitates slim graphite to the nickel metal side adjoining the laminated pearlite matrix (Fig. 12c) with flake graphite in the HAZ. Between the circumference and both edges, the nickel–martensite with slim graphite on the nickel metal side, adjoins the laminated pearlite matrix which contains slender flake graphite and precipitated eutectic graphite due to a small enlarged portion of fusion of the base metal. In the centre of the bead, the HAZ has a laminated pearlite structure containing flake graphite, but at the edges of the bead, the HAZ includes a eutectic graphite–crystallized layer containing slender flake graphite and a laminated pearlite layer. In this case, the HAZ is comprised of eutectic graphite–precipitated layer and a relatively thick pearlite layer, which is a structure which has a marked effect on graphitization.

Finally, the diffusion of nickel in the deposit metal into the HAZ will be discussed. It may be important to consider whether the solute in the filler metal can actually diffuse into the HAZ or not. In the welding of cast iron, the liquid portion of the HAZ is easy to freeze as white iron. Therefore, the chemical composition of the liquid is altered by means of diffusion of the element in the deposit metal into the HAZ and formation of white iron may be anticipated and thus avoided. Figs. 8 and 9 show EPMA traces which nickel diffuses up to the ledeburitic layer in the HAZ. On deposition of the filler metal, the partial base metal in the vicinity of the deposit metal begins to melt due to the heat from the deposit metal side, and an interaction between the deposit metal and the partially fused metal may play an important role in diffusion of nickel into the HAZ. Accordingly, diffusion of nickel from the deposit

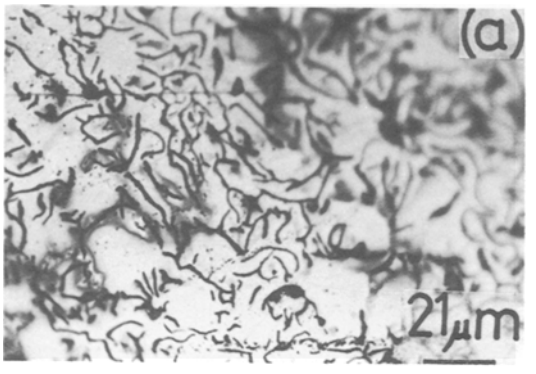

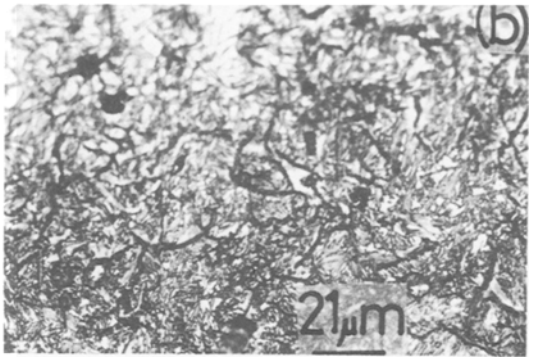

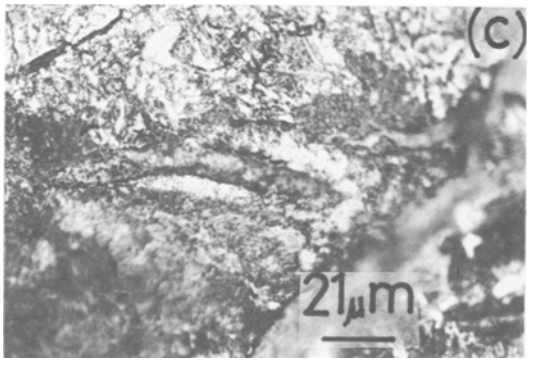

Figure 12 Microstructure of deposited fusion boundary area of FGI with CIA-1 welding rod produced by a plasma arc using argon plasma gas and Ar + 10% H_2 shielding gas at an arc current of 130 A. Nital etch. (a) Many slim graphites within the nickel austenitic matrix in the deposit metal. (b) Nickel–martensite and slim graphite in the fusion boundary region. (c) Finely laminated pearlite matrix adjacent to the nickel–martensite.

metal into the HAZ occurs at least up to the fused base metal of the HAZ.

5. Conclusions

Microstructural changes produced by a plasma arc local-melting method in the fusion region of deposited metal, fusion boundary region and the HAZ of flake graphite cast iron were investigated, and the principal results and conclusions are as follows:

1. In the absence of filler metal, the structure of the fusion region is that of a hypoeutectic white cast iron at the centre and of fine ledeburite in the vicinity of fusion line.

2. In the fusion boundary region where a supercooling phenomenon occurs, fine martensite precipitates along the fusion line for a small heat input and secondary graphite precipitates for a large heat input.

3. The HAZ is composed of white martensitic, dark martensitic and martensitic–fine pearlitic layers after a small heat input, and of laminated pearlitic and laminated pearlitic–ferritic layers after a large heat input.

4. The solid solution of carbon from flake graphite into the matrix occurs mostly in the HAZ and no evidence of fusion due to a partial lowering of the melting point of the matrix adjacent to the flake graphite can be found.

5. Using filler metal, the structure of deposit metal is that of nickel austenitic matrix precipitating tiny graphite nodules or slim graphite for nickel and Ni–Fe filler metals and that of a pearlitic matrix for iron filler metal.

6. In the fusion boundary region, nickel–martensite, eutectic or slim graphite, fine nickel–martensite precipitates with a nickel system filler metal and a columnar structure of ferrite and pearlite exists for the iron filler metal.

7. The HAZ is composed of four layers, i.e. ledeburitic, martensitic, martensitic–fine pearlitic and laminated pearlitic, for nickel filler metal, of two layers, i.e. ledeburitic and laminated pearlitic, for Ni–Fe filler metal, and of three layers, i.e. ledeburitic, eutectic graphite and laminated pearlitic for the iron filler metal. The structure of the HAZ is thought to be altered by the melting point of the filler metal.

8. The ledeburitic layer in the HAZ is thicker for iron filler metal than for nickel or Ni–Fe filler metal because of the difference in freezing points of the filler matrix.

9. The hardness of the nickel–martensite and ledeburitic layers in the fusion boundary region is very high; however, it is slightly lower in the ledeburitic area when iron filler metal is used.

10. The formation of ledeburitic and martensitic layers can be avoided by a relatively longer arc-time, that is, larger heat input, and by the use

of a filler metal having a melting point close to that of the base metal.

11. It is obvious from the presence of a nickel concentration gradient in the ledeburitic layer that the diffusion of nickel from the deposit metal to the HAZ occurs at least up to the fused base metal in the HAZ.

Acknowledgements

The author would like to thank Mr H. Yamaguchi (Hitachi Ltd) for his help and advice in the plasma arc experiment, Messrs S. Yamada, K. Enami and K. Wako for the preparation of the specimens and the filler metals, Mr S. Oki for the EPMA work and Mr S. Takeyama for element analysis.

References

1. YOUNG-WON KIM, R. R. STRUTT and H. NOWOTNY, *Met. Trans.* **10A** (1979) 881.
2. P. R. STRUTT, *Mater. Sci. Eng.* **49** (1981) 87.
3. W. HILLER, *Giesserei* **63** (1976) 316.
4. M. J. TOMSIC and C. E. JACKSON, *Weld. J.* **53** (1974) 109s.
5. B. TOWNSHEND and E. O. PORTER, *ibid.* **38** (1959) 329s.
6. M. HOMMA, T. WADA and K. YAMAYA, *Sci. Rep. RITU* **12A** 1960) 437.
7. J. H. DEVLETIAN, *Weld. J.* **57** (1978) 183s.
8. *Idem, ibid.* **59** (1980) 349s.
9. T. ISHIDA, *J. Mater. Sci.* **18** (1983) 1773.
10. M. HOMMA and T. ISHIDA, *Sci. Rep. RITU* **17A** (1965) 1.
11. B. J. ECK, "Metal Handbook, Properties and Selection: Iron and Steels", Vol. 1, 9th Edn. (American Society for Metals, Ohio, 1978) Cast Iron/13.
12. H. THIELSCH, *Weld. J.* **31** (1952) 37s.
13. W. ZITZELSBEGER, *Schwei. Schnei.* **11** (1959) 416.
14. J. RUGE and W. ZITZELSBERGER, *ibid.* **10** (1958) 86.
15. T. KASE, *Sci. Rep. RITU* **14** (1925) 173.
16. M. OKAMOTO and R. YODA, "Atlas of Microstructures-Cast Iron" (Yokendo Press, Tokyo, 1961).
17. T. ISHIDA, *J. Mater. Sci.* **19** (1984) 3800.
18. W. HUME-ROTHERY, "The Structures of Alloys of Iron" (Pergamon Press, Oxford, 1966) p. 253.
19. H. IKAWA, S. SHIN, Y. NAKAO and K. NISHIMOTO, *J. Jap. Weld. Soc.* **44** (1975) 229.
20. R. D. WASSERMAN, J. F. QUAAS and J. P. BRODERICK, *Weld. J.* **36** (1957) 481.
21. J. SOHN, W. BOAM and H. FISK, *ibid.* **32** (1953) 823.

Received 18 January
and accepted 13 March 1984